

ABOUT THE GENERATION OF UNSTRUCTURED MESH FAMILIES FOR GRID CONVERGENCE ASSESSMENT BY MIXED MESHES

JOCHEN WILD*

* German Aerospace Center (DLR)
Institute of Aerodynamics and Flow Technology
Lilienthalplatz 7, 38108 Braunschweig, Germany
e-mail: jochen.wild@dlr.de, <http://www.dlr.de/as>

Key words: Grid Generation, Unstructured Meshes, Anisotropic Meshes, Mixed Meshes, CFD.

Abstract. This work describes properties of the mixed mesh approach that are especially suitable for generating families of meshes to assess the grid refinement convergence of CFD solvers. The paper outlines how a regular grid refinement is achieved throughout the domain. The distributions of characteristic grid quality metrics are compared and a grid convergence study is outlined for a commonly used case for outer aerodynamics, the Boeing CRM configuration of the 5th AIAA Drag Prediction Workshop.

1 INTRODUCTION

The assessment of the accuracy of a simulation method is a crucial step during the verification and validation process of the simulation software. Even the best mathematically derived formulation has to prove the rate of convergence with increasing mesh resolution for designated applications.

For applications of CFD for aerodynamics of aircrafts a series of five workshops has been organized under the governance of the American Institute of Aeronautics and Astronautics (AIAA) [1]. A major focus of the comparisons of solvers for simulation accuracy was laid on the grid convergence, for which families of grids have been provided, both structured and unstructured ones. A major conclusion of all workshops has been the highly demanding generation of unstructured mesh families.

While for structured meshes the generation of self-similar grids with different but regularly refined grid resolutions is straight forward, for unstructured hybrid meshes this is a more complicated task. Due to the – in most cases – fully automatic generation a distinct control on local mesh resolution and its influence into other parts of the mesh is hard to control.

This paper outlines the usability of the mixed mesh approach for the purpose of generating families of meshes for grid convergence assessment. Block-unstructured mixed meshes provide structured meshes in the near field of the aerodynamic body where viscous effects dominate and a high resolution normal to the wall is needed. In contrast to pure block-structured meshes, limitations of topologies are overcome by locally using unstructured mesh element types, mainly prismatic elements. For the outer field an a priori defined anisotropic

field triangulation is applied to allow for maximum flexibility and to minimize the effort of user input.

2 THE MIXED MESH FRAMEWORK

The meshing framework used is the formerly structured multi-block grid generation MegaCads developed at DLR [2]. In recent years unstructured capabilities have been introduced. Among these are a parabolic marching procedure to generate prismatic layers based on the same mathematical approach as used in the elliptic smoothing of structured blocks [3], the linking to a number of volume triangulation codes including the SIMMETRIX software [4] used within this work, and a memory efficient way to specify a priori a smooth anisotropic metric field for the triangulation smoothly adopting to the underlying structured and quasi-structured elements [5].

2.1 Mixed mesh approach

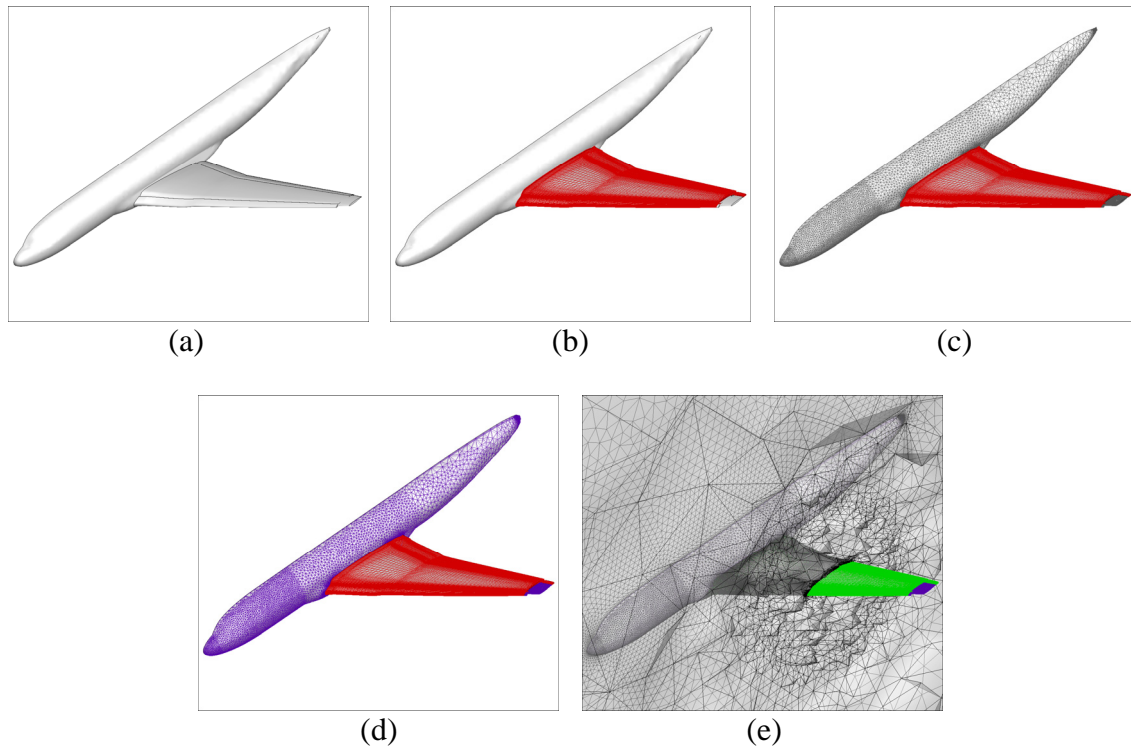


Figure 1: Generating a mixed mesh: (a) surface description; (b) structured hexahedral grids for boundary resolution; (c) surface triangulation of remaining geometry parts; (d) extrusion of prismatic layers; (e) anisotropic field triangulation

The big shortcoming of hybrid unstructured grids is the low anisotropy of surface triangles resulting in a large number of grid points, which is agglomerated through the number of prismatic layers for the boundary layer resolution. This low anisotropy leads to an unnecessary high resolution in span direction, especially for high aspect ratio wings. Recovering the experience with the application of structured grids, it is known, that the aspect ratios of the surface quadrilaterals can be much higher, additionally resulting in well aligned

body conforming meshes. The shortcoming of an overall use of structured meshes is the increasing complexity of the targeted configurations, where structured meshing reaches its limitations, mainly due to grid topology issues.

The simple idea of mixed meshes is to make as much use as possible of the advantages of structured meshes skipping the disadvantages of complicated topology generation. In **Figure 1** the general procedure is sketched for a transport aircraft high-lift configuration. Boundary layer regions are meshed by structured hexahedral mesh blocks, except when the topology gets difficult to be generated. The advantageous C-type meshes for wake resolutions are used here as far as possible. Whenever the block-structured topology gets too complicated, the mixed mesh approach switches to unstructured elements. For the remaining parts of boundary layer regions near surfaces, quasi-structured prismatic elements are used. For the outer flow field the volume is filled by tetrahedrons.

In the past the author showed that mixed meshes significantly reduce mesh sizes without reduction of accuracy [6],[7]. Since the methods work flow starts with the block-structured meshes, the generation method is best described as block-unstructured mixed mesh method. Also commercial grid generation software in the meantime has implemented mixed meshing capabilities, e.g. ICEM CFD [8] and PointWise [9], but those methods rely on isotropic triangulation methods.

2.2 Mixed mesh family around Boeing CRM

Figure 2 shows a view on the grid family around the Boeing Common Research Model (CRM) [10] in the configuration without tail as used in the 5th Drag Prediction Workshop. The coloring depicts the different types of grid elements. For the grid family, three levels of different mesh density have been generated using the anisotropic mixed meshing approach. The number of cells in the structured part is multiplied by a factor of 1.5 for adjacent grid levels in each direction, while the cell sizes are reduced by the same magnitude wherever specified. The portion of the fluid volume meshed by structured elements is not changed in order to obtain self-similar meshes.

The used method derives a smooth anisotropic metric field based on the anisotropy of the adjacent structured hexahedrons and quasi-structured prisms. This anisotropic metric field is inherently responsible to achieve the self-similarity and grid family properties in the unstructured domain of the meshed volume, since all information of grid resolution is directly derived from the structured and quasi-structured grid parts.

Table 1: Characteristics of the mesh family around the Boeing CRM configuration

CRM mesh size	coarse	scaling ↔	medium	scaling ↔	fine
grid points	1,368,229	2.68	3,666,721	2.85	10,450,269
surface triangles	38,548	2.20	84,686	2.20	186,370
surface quadrilaterals	27,753	2.24	62,680	2.28	142,134
tetrahedrons	4,222,454	2.19	9,267,026	2.18	20,276,862
Prisms	340,935	3.16	1,078,816	3.26	3,513,840
hexahedrons	419,756	3.46	1,452,208	3.46	5,019,198

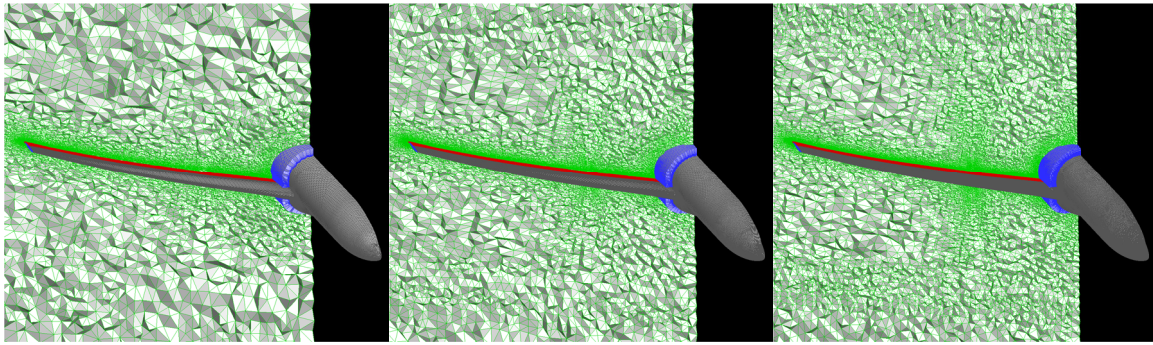


Figure 2: Family of grids around the Boeing CRM configuration, left to right: coarse – medium – fine; colors indicate cell type: red=hexahedrons, blue=prisms, green=tetrahedrons

In **Table 1** some characteristic features with respect to grid family properties are shown. The number of surface elements scales between the grid levels close to the theoretical value of $1.5^2=2.25$. Prisms and hexahedrons counts scale also close to the theoretical value of $1.5^3=3.375$. Interestingly, the scale of the number of tetrahedrons is close to the theoretical value for surface elements. Therefore, also the overall point number scales less than theoretically expected or achieved in pure structured meshes. But, interestingly the inverse of the point number to the power of two-third, which is later used for Richardson extrapolation, scales almost exactly by a factor of 2 between grid levels, thus indicating a doubling of grid density.

3 GRID CONVERGENCE OF THE BOEING CRM CASE

3.1 Grid quality indicators

The selection of indicators for a priori grid quality assessment has to respect the type of solver later on used for the simulation. For finite element methods (FEM) most commonly used are indicators that look for the shape of single elements and detecting badly shaped cells like slivers, needles, and hats that inherently disrupt the numerical accuracy of the solution. For the targeted finite volume (FVM) flow solver these element based metrics are of less significance since for the flux computations needed the relationship of neighboring elements is at least as important. Knupp [11] introduced algebraic grid quality metrics based on the Jacobian of elements, which are the transformation matrices from computational into physical space. They are more representative, since the averaging of the cell based Jacobians for a common grid node provide an indication for the smoothness of the surrounding cells. In the following two of the metrics provided by Knupp’s MESQUITE library are used to show the comparability of the generated grids in the sense of self-similarity for a family of grids.

Figure 3 shows the histogram of the variations of the “local size” quality metric for the three generated meshes around the Boeing CRM. A value of one indicates that all elements surrounding a grid node have the same size. The counts of grid nodes in the histogram are normalized by the number of overall grid points and are plotted on a logarithmic axis to more precisely inspect the behavior of the different grid levels at values of the lower quality metric values. The figure shows that the distributions of the “local size” quality metric is nearly

identical for all three mesh levels indicating that the characteristics of the grid are not depending on the grid size in this respect.

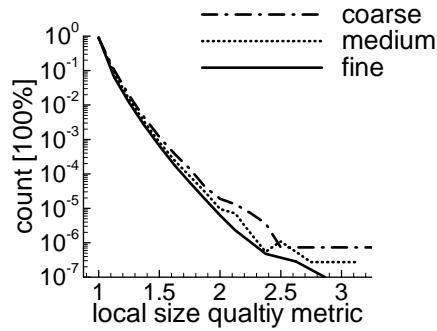


Figure 3: histograms of local size variation of the cells around a grid node for three mesh levels of the grids around the Boeing CRM.

Figure 4 shows a histogram for the vertex based condition number, which is an average of the condition numbers of the Jacobians of the elements surrounding a grid node. Since the targeted meshes are anisotropic high values of are expected since the value directly reflects the anisotropy of the grid. The histogram shows that the generated grids show similar distributions of anisotropy in the mesh and therefore the needed self-similarity.

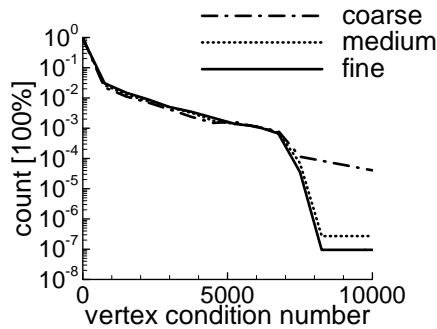


Figure 4: Histogram of the vertex based condition number variation for three mesh levels of the grids around the Boeing CRM.

Another important indicator of the suitability of a grid for CFD is the local number of neighbors to a grid node. Meshes often degrade the simulation quality by having local hot-spots of the neighboring node count. Especially hybrid meshes where the anisotropy of quasi-structured cells is not respected can have up to 200 neighboring nodes and the flux computations are comprised by this. **Figure 5** shows the distribution of the number of neighboring nodes and – again – shows that the characteristics of the three mesh levels are very similar.

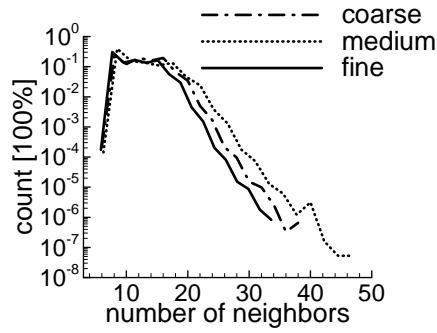


Figure 5: Histogram of the variation of the number of neighbors of a grid node for three mesh levels of the grids around the Boeing CRM.

3.2 Grid convergence assessment

The assessment of the grid convergence is calculated using the DLR TAU-code [12], a second order finite volume CFD solver. The assessment is made based on overall aerodynamic characteristics and on the contributions of local parts to show the suitability of the mixed mesh approach for such studies in global and local effects. Data for comparison is included from wind tunnel tests in the NASA National Transonic Facility [13] and from the result of the 5th AIAA Drag Prediction Workshop (DPW5) [14].

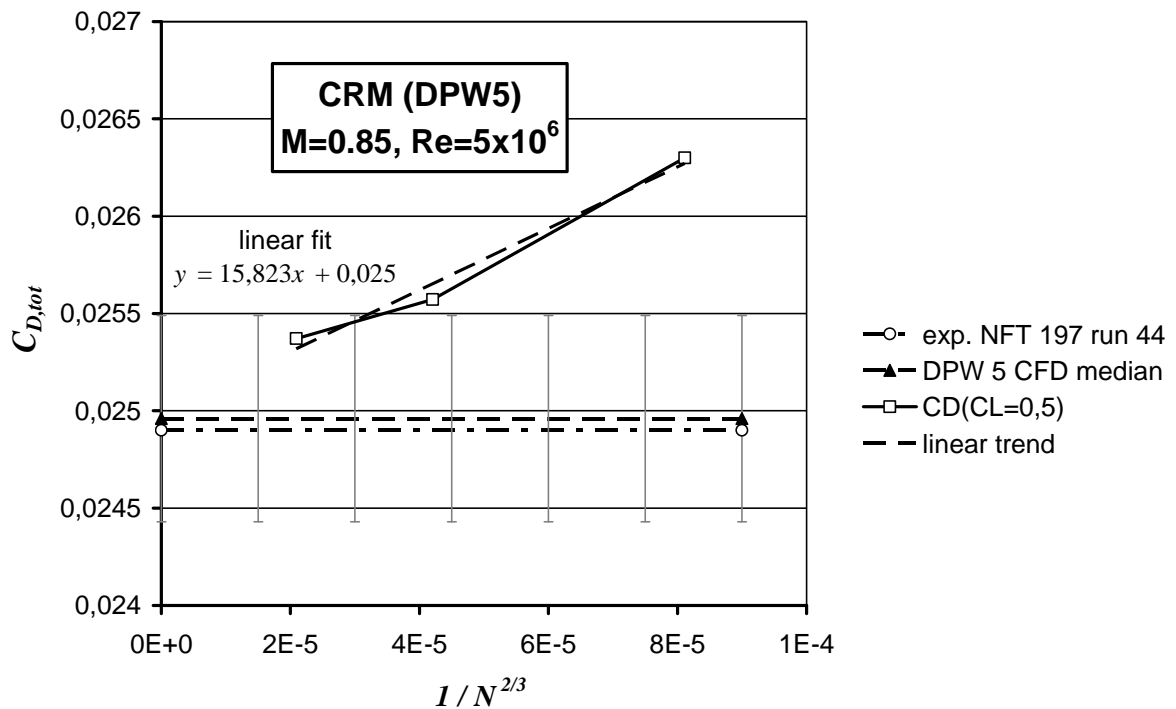


Figure 6: Grid convergence of the total drag coefficient compared to experimental data and the average of CFD calculations performed for the 5th AIAA Drag Prediction Workshop.

Figure 6 shows the grid convergence of the overall drag coefficient compared to experimental data and the average result of DPW5. The value of the drag coefficient is plotted against the inverse of the number of nodes to the power of two-third, according to the Richardson extrapolation for 2nd order CFD codes. Along with the average the standard deviation of the CFD results is shown by error bars. It should be highlighted that the error bar is also derived from the values obtained by Richardson extrapolation to infinite grid density. It is worth to highlight that for the presented meshing strategy already the medium mesh is only slightly off the standard deviation of the CFD calculations and the extrapolated value of the drag coefficient ($C_D = 0.0250$) is only 0.4% off the experimental value. The comparison of the drag coefficients for the distinct grid refinements shows a slight deviation from the theoretical 2nd order behavior of the CFD method.

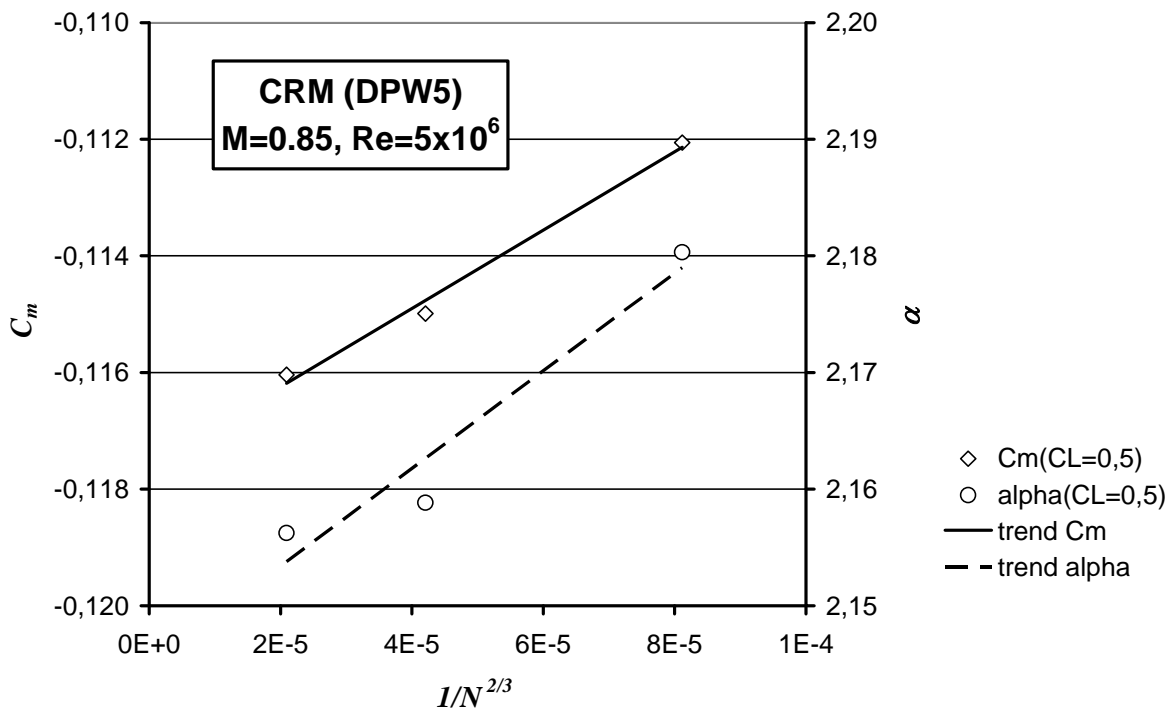


Figure 7: Grid convergence of the pitching moment coefficient and the angle of attack.

Figure 7 shows the grid convergences of the pitching moment coefficient and the angle of attack to obtain a lift coefficient of $C_L = 0.5$. Experimental data is omitted here, since already in the description of DPW5 a large deviation between CFD and experiment was observed. An evaluation of the CFD results similar to the analysis of the drag coefficient is not available, but from the data available it is confirmed that both characteristics fall well into the scatter of CFD results. The pitching moment shows a similar accordance to the 2nd order trend as the drag coefficient, while the angle of attack shows a larger deviation from a 2nd order behavior.

There are in a first view two aspects that can be addressed to more deeply analyze the slight deviation from the theoretical grid convergence in order to see whether the mesh sequence is well suited for the grid convergence study. First, it is worth to differentiate

between the partial contributions the total aircraft drag is composed from. **Figure 8** shows the grid convergence of the drag coefficient separated into pressure and viscous parts. Comparing the trend lines against the distinct values there is no obvious difference in the behavior between the two principal contributors to the overall drag coefficient. This result is especially important to conclude on the meshing strategy to generate the grid family. The grid refinement regarding the structured and quasi-structured parts to resolve the viscous layers of the flow behave the same way, otherwise the grid convergence of the distinct contributions to the drag coefficient would show a behavior different from the pressure part.

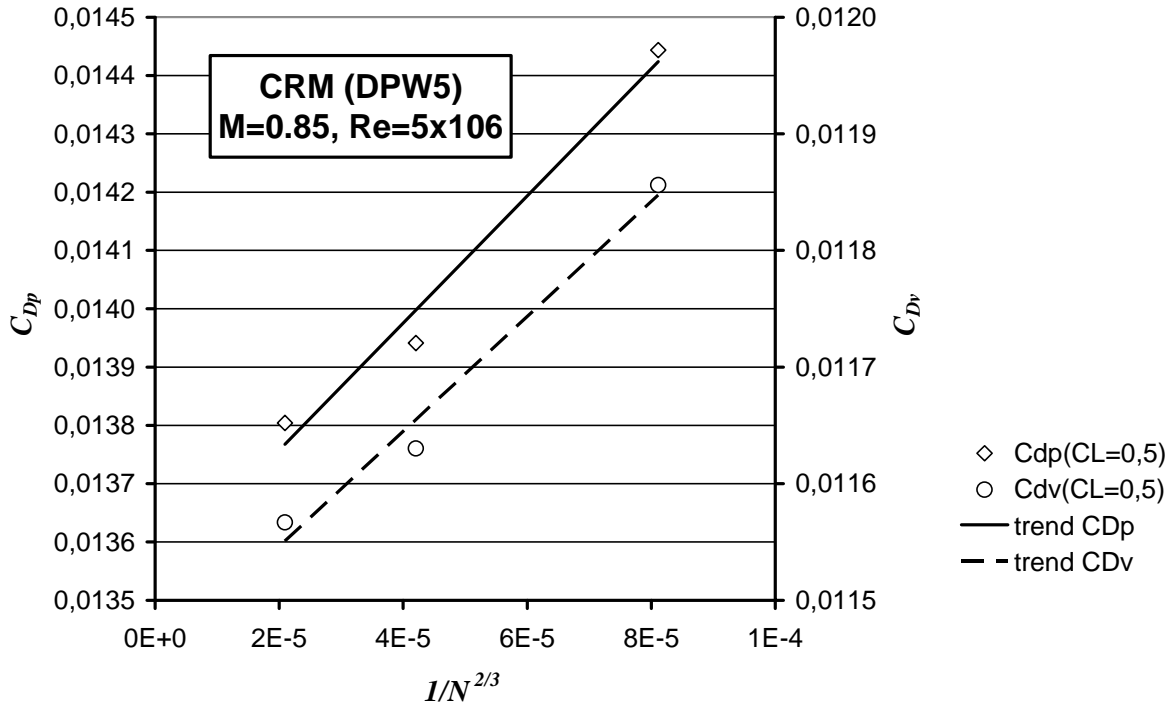


Figure 8: Grid convergence of the drag coefficient divided into pressure and viscous parts.

The second influence to analyze concerns the contribution of the different model bodies to the overall drag estimate. In terms of the meshing strategy this reflects the choice of structured hexahedrons or quasi-structured prisms. **Figure 9** shows the drag split for the two bodies, wing and fuselage respectively. As formerly described, the wing surrounding aside the most outboard wingtip is meshed with structured hexahedrons including the wake of the wing while the fuselage is covered by layers of prismatic cells. The figure shows that the deviation from the ideal 2nd order trend line is significantly larger for the fuselage body, while the wing is very close to the 2nd order behavior. This result is not as astonishing as the grid conformity between grid levels can be easily achieved for the structured parts, which includes the complete structured mesh parts as well as the quasi-structured direction of the prism stacks. So this result is not contradictory to the missing influence of the mesh type on the previous shown differentiation between pressure and viscous parts. The behavior observed here highlights that the self-similarity is already limited to some extent within the surface

triangulation of the body.

The behavior observed for the drag coefficient is even more pronounced regarding the contributions of the different bodies to the pitching moment coefficient shown in **Figure 10**. For the contribution of the wing the grid convergence shows a nearly exact 2nd order behavior. It can be therefore concluded that the deviation from the theoretical order can be attributed mainly to the contribution of the fuselage. This confirms the observations obtained for the drag coefficient even more pronounced.

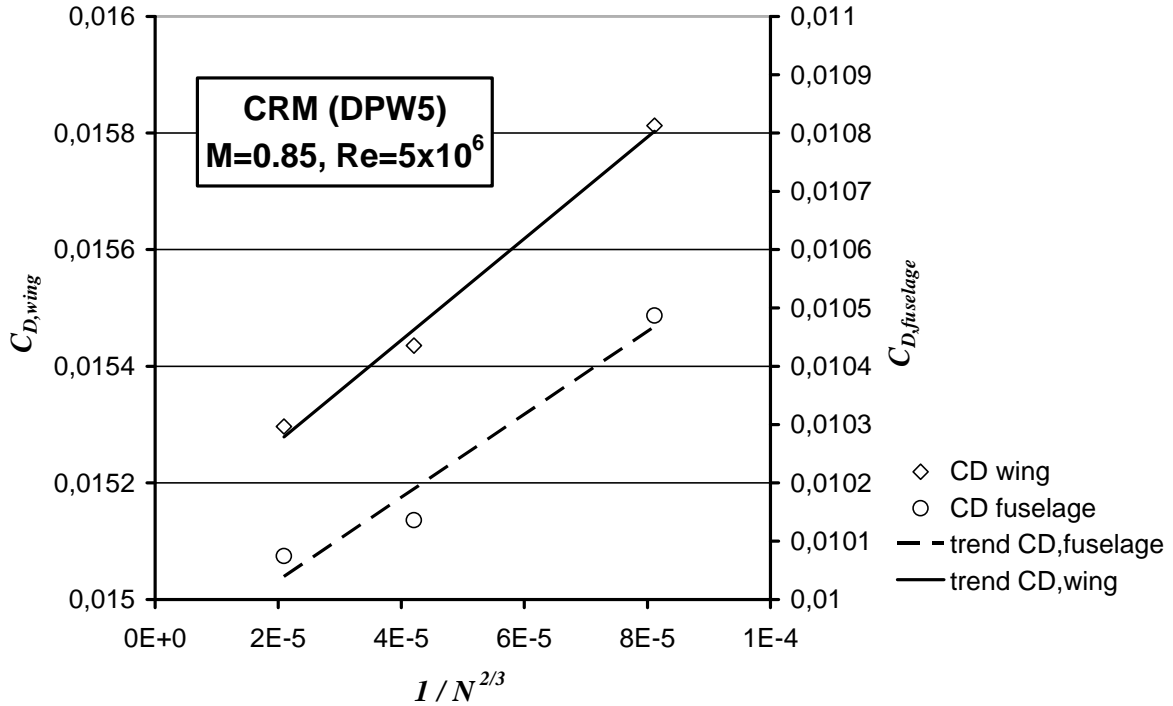


Figure 9: Grid convergence of the drag coefficient separated to contributions of wing and fuselage.

It can be concluded that the formal conformance of grid levels for a grid family can be obtained by the presented meshing approach, but special attendance must be paid to the unstructured parts of the mesh. The generated mesh family fulfills the requirements for a grid convergence study. The results confirm that a basic recommendation for the grid size require that the number of surface element and unstructured tetrahedrons scale with a power of 2 between the grid levels, while the number of structured and quasi-structured elements scale with the power of 3 depending on the refinement ratio.

4 CONCLUSIONS

The mixed meshing approach allows for the generation of mesh families for the assessment of grid convergence behavior of CFD solvers. The use of block-structured cells in near wall regions inherently possesses this capability. The derivation and usage of an adjacent smooth anisotropic metric field for the flow field triangulation promotes the self-similarity of the

structured part of the mesh into the unstructured part. Nevertheless, the result obtained for the differentiation between wing and fuselage indicates that the appropriate meshing of the fuselage is not negligible for the accuracy of the CFD simulation of wing body configurations.

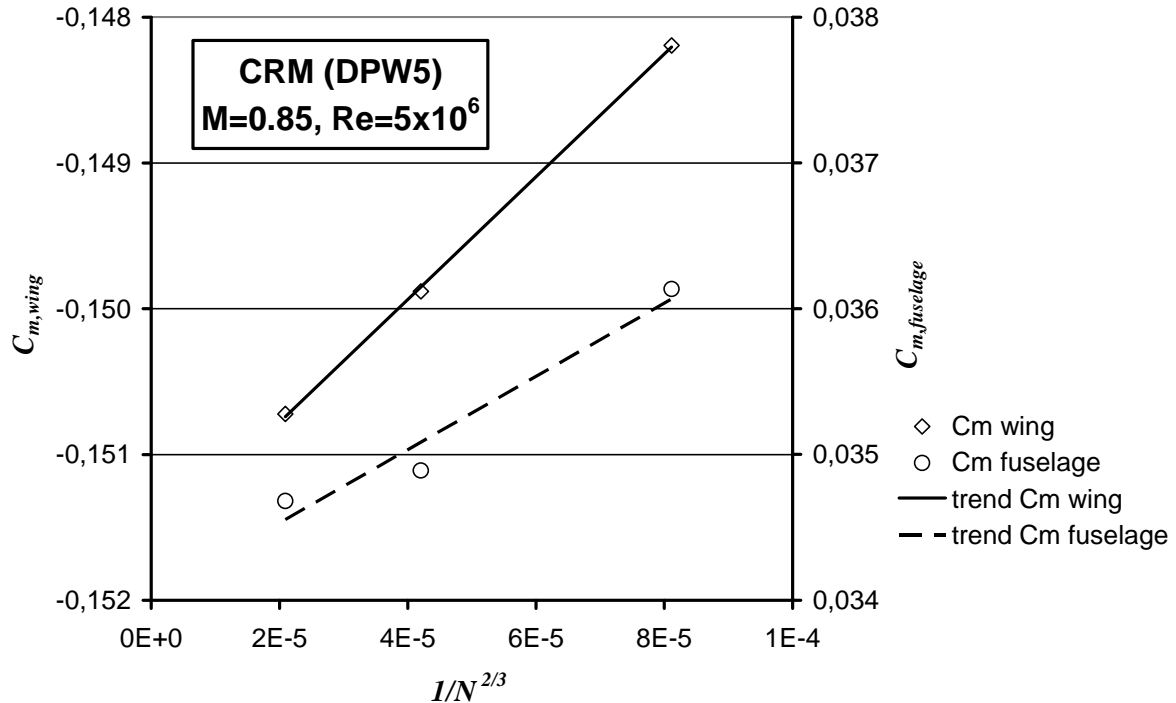


Figure 10: Grid convergence of the pitching moment coefficient separated to contributions of wing and fuselage

REFERENCES

- [1] Mavriplis, D.J., Vassberg, J.C., Tinoco, E.N., Mani, M., Brodersen, O., Eisfeld, B., Wahls, R.A., Morrison, J.H., Zickuhr, T. Levy, D., and Murayama, M. "Grid Quality and Resolution Issues from the Drag Prediction Workshop Series", *AIAA Journal of Aircraft* 2009 **46**(3):935-950.
- [2] Brodersen, O., Hepperle, M., Ronzheimer, A., Rossow, C.-C. and Schöning, B. "The Parametric Grid Generation System MegaCads", *Proceedings 5th International Conference on Numerical Grid Generation in Computational Field Simulation*, National Science Foundation, (1996), pp. 353-362.
- [3] Wild, J. Application Of Smooth Mixed Meshes Based On Metric Identity In Aerospace Analysis And Design. In: Grimella RV (ed) *Proceedings of the 17th Int. Meshing Roundtable*, Springer, Berlin Heidelberg, (2008), pp. 387-398.
- [4] Simmetrix Inc., <http://www.simmetrix.com>, v8.0 -130213, (accessed 2013)
- [5] Wild, J. 3D Anisotropic Delaunay Meshing for Ideal Interfacing to Block-Unstructured Mixed Meshes using a Sparse Octree for Metric Size Propagation. *European Congress on Computational Methods in Applied Sciences and Engineering (ECCOMAS 2012)* proceedings on CD-ROM (2012) paper no. 2541.

- [6] Wild, J. Acceleration of Aerodynamic Optimization Based on RANS-Equations by Using Semi-Structured Grids, in K.C. Giannakoglou, W. Haase (eds.) *ERCRAFT Design Optimization: Methods & Applications*, conference proceedings on CD-ROM (2004).
- [7] Wild, J. Smooth Mixed Meshes for Acceleration of RANS CFD in Aircraft Analysis and Design, *48th AIAA Aerospace Science Meeting and Exhibit* (2011) AIAA-2011-1267.
- [8] Ansys Inc. Home > Products > ANSYS ICEM CFD. <http://www.ansys.com/> (accessed 2013).
- [9] Pointwise Inc. Pointwise's Unstructured and Hybrid Meshing. <http://www.pointwise.com/> (accessed 2013).
- [10] Vassberg, J.V., DeHaan, M.A., Rivers, S.M. and Wahls, R.A. Development of a Common Research Model for Applied CFD Validation Studies. *26th AIAA Applied Aerodynamics Conference*. (2008) AIAA-2008-6919,.
- [11] Knupp, P.M. Algebraic Mesh Quality Metrics. *SIAM Journal of Scientific Computing* (2001) **23**(1):193-218.
- [12] Schwamborn, D., Gerhold, Th. and Heinrich, R. The DLR TAU-Code: Recent Applications in Research and Industry. *ECCOMAS CFD 2006*, proceedings on CD-ROM (2006).
- [13] Rivers, M. and Dittberner, A. Experimental Investigations of the NASA Common Research Model in the NASA Langley National Transonic Facility and NASA Ames 11-Ft Transonic Wind Tunnel. *49th Aerospace Sciences Meeting* (2011) AIAA 2011-1126. Data on Common Research Model available at <http://commonresearchmodel.larc.nasa.gov/>, (accessed March 2013).
- [14] Levy, D.W., Laflin, K.R., Tinoco, E.N., Vassberg, J.C., Mani, M., Rider, B., Rumsey, C.L., Wahls, R.A., Morrison, J.H., Brodersen, O.P., Crippa, S., Mavripilis, D.J. and Murayama, M. Summary of Data from the Fifth AIAA CFD Drag Prediction Workshop. *51st AIAA Aerospace Sciences Meeting* (2013) AIAA 2013-0046.